SDSS J102111.02+491330.4: A NEWLY DISCOVERED GRAVITATIONALLY LENSED QUASAR[1]

BART PINDOR,[2,3] DANIEL J. EISENSTEIN,[4] MICHAEL D. GREGG,[5,6] ROBERT H. BECKER,[5,6] NAOHISA INADA,[7] MASAMUNE OGURI,[8,9]
PATRICK B. HALL,[10] DAVID E. JOHNSTON,[9] GORDON T. RICHARDS,[9] DONALD P. SCHNEIDER,[11] EDWIN L. TURNER,[9]
GUIDO BRASI,[4] PHILIP M. HINZ,[4] MATTHEW A. KENWORTHY,[4] DOUG MILLER,[4] J. C. BARENTINE,[12]
HOWARD J. BREWINGTON,[12] J. BRINKMANN,[12] MICHAEL HARVANEK,[12] S. J. KLEINMAN,[12]
JUREK KRZESINSKI,[12,13] DAN LONG,[12] ERIC H. NEILSEN, JR.,[14] PETER R. NEWMAN,[12]
ATSUKO NITTA,[12] STEPHANIE A. SNEDDEN,[12] AND DONALD G. YORK[15]

ABSTRACT

We report follow-up observations of two gravitational lens candidates identified in the Sloan Digital Sky Survey (SDSS) data set. We have confirmed that SDSS J102111.02+491330.4 is a previously unknown gravitationally lensed quasar. This lens system exhibits two images of a $z = 1.72$ quasar, with an image separation of $1\farcs14 \pm 0\farcs04$. Optical and near-IR imaging of the system reveals the presence of the lensing galaxy between the two quasar images. Observations of SDSS J112012.12+671116.0 indicate that it is more likely a binary quasar than a gravitational lens. This system has two quasars at a redshift of $z = 1.49$, with an angular separation of $1\farcs49 \pm 0\farcs02$. However, the two quasars have markedly different spectral energy distributions, and no lens galaxy is apparent in optical and near-IR images of this system. We also present a list of 31 SDSS lens candidates that follow-up observations have confirmed are *not* gravitational lenses.

Key words: gravitational lensing — quasars: general

1. INTRODUCTION

The fortuitous alignment of the gravitational potential of a foreground galaxy with a background quasar can cause multiple images of the quasar to be seen. These rare systems can be used to probe the mass distribution of the lens galaxy (Kochanek 1995), measure the Hubble constant through time delay measurements (Refsdal 1964; Kundic et al. 1997; Koopmans & Fassnacht 1999), and constrain cosmological models through the use of lensing statistics (Turner 1990; Fukugita et al. 1990; Chae et al. 2002; Kuhlen et al. 2004). For a comprehensive review of the principles and applications of strong lensing, the reader is referred to Kochanek et al. (2006). Newly discovered lens systems can be of interest both for individual study and as additional data points in studies of lens ensembles. In some cases, lens samples can be used to draw statistical inferences without particular regard to how the lenses were selected (e.g., Treu & Koopmans 2004; Rusin & Kochanek 2005), but studies that consider properties of the lens population, such as the distribution of image separations (e.g., Li & Ostriker 2002; Chae & Mao 2003) or the quad fraction (Cohn & Kochanek 2004), would benefit from a sample defined by a clearly understood selection procedure, so as to allow for the correction of selection effects. To date, the best-defined sample is that produced by the radio Cosmic Lens All-Sky Survey (CLASS) (Myers et al. 2003). However, the fact that only ~10% of quasars are radio-loud (Ivezić et al. 2002) implies that optical surveys offer the best future prospect for assembling large statistical samples.

The Sloan Digital Sky Survey (SDSS; York et al. 2000) data set provides an excellent opportunity to discover gravitationally lensed quasars. The $\sim10^4 \ \mathrm{deg}^2$ of five-band photometry and the spectroscopic sample of $\sim10^5$ quasars should allow for the compilation of a lensed quasar sample that is both large and statistically well defined in comparison to existing optical samples. The parent sample of SDSS quasars is selected by a single, clearly defined algorithm (Richards et al. 2002) and the uniform image processing pipeline allows for geometric selection effects to be accurately characterized through the use of image simulations (Pindor et al. 2003, hereafter P03). To date, the SDSS has discovered several galaxy-scale lenses (e.g., Johnston et al. 2003; Pindor et al. 2004), as well as the largest known quasar lens (Inada et al. 2003). In this work, we report follow-up observations of two objects identified as promising lens candidates during an MMT spectroscopic run. We also present a list of objects that have been ruled out as gravitational lenses during our ongoing search for lensed quasars in the SDSS data set.

2. OBSERVATIONS

2.1. *SDSS Technical Summary*

The SDSS is a photometric and spectroscopic survey across 10,000 deg^2 of the northern Galactic cap using the 2.5 m SDSS

[2] Department of Astronomy, University of Toronto, 60 St. George Street, Toronto, ON M5S 3H8, Canada.
[3] Canada-France-Hawaii Telescope Legacy Survey Postdoctoral Fellow.
[4] Steward Observatory, University of Arizona, 933 North Cherry Avenue, Tucson, AZ 85721.
[5] Physics Department, University of California, 1 Shields Avenue, Davis, CA 95616.
[6] Institute of Geophysics and Planetary Physics, Lawrence Livermore National Laboratory, L-413, 7000 East Avenue, Livermore, CA 94550.
[7] Institute of Astronomy, University of Tokyo, 2-21-1 Osawa, Mitaka, Tokyo 181-0015, Japan.
[8] Department of Physics, University of Tokyo, Hongo 7-3-1, Bunkyo-ku, Tokyo 113-0033, Japan.
[9] Princeton University Observatory, Peyton Hall, Princeton, NJ 08544.
[10] Department of Physics and Astronomy, York University, 4700 Keele Street, Toronto, ON M3J 1P3, Canada.
[11] Department of Astronomy and Astrophysics, Pennsylvania State University, University Park, PA 16802.
[12] Apache Point Observatory, 2001 Apache Point Road, P.O. Box 59, Sunspot, NM 88349-0059.
[13] Mount Suhora Observatory, Cracow Pedagogical University, ul. Podchorazych 2, 30-084 Krakow, Poland.
[14] Fermi National Accelerator Laboratory, P.O. Box 500, Batavia, IL 60510.
[15] Department of Astronomy and Astrophysics, University of Chicago, 5640 South Ellis Avenue, Chicago, IL 60637.

telescope at Apache Point Observatory. SDSS imaging is carried out with a wide-field camera (Gunn et al. 1998) that makes nearly simultaneous observations of objects in five passbands: u, g, r, i, and z. Together, the passbands cover the optical wavelengths from the atmospheric cutoff in the blue to the minimum detectable energy for the silicon CCDs in the red (Fukugita et al. 1996). Photometric calibration of the imaging survey is separately carried out by an automated 0.5 m telescope that monitors a set of standard stars (Smith et al. 2002) while photometric data are being acquired (Hogg et al. 2001). The position of the stellar locus can be used to independently verify the accuracy of the photometric zero-point calibrations (Ivezić et al. 2004). The SDSS imaging camera also incorporates astrometric CCDs that provide astrometry of detected objects with an accuracy typically better than $0''.1$ (Pier et al. 2003). SDSS spectroscopy is carried out on the same telescope by two fiber-fed double spectrographs that produce spectra with a resolution ($\lambda/\Delta\lambda$) of $\sim$2000 covering the wavelength range 3800–9200 Å. Together, the spectrographs have 640 fibers that are assigned based on previous SDSS imaging through an efficient tiling algorithm (Blanton et al. 2003). For more comprehensive documentation of the survey, readers are encouraged to consult Stoughton et al. (2002) and Abazajian et al. (2003, 2004, 2005).

2.2. Selection as Lens Candidates

Five-band photometry of SDSS J102111.02+491330.4 (hereafter SDSS J1021+4913) and SDSS J112012.12+671116.0 (hereafter SDSS J1120+6711) was obtained in the course of normal SDSS imaging on 2001 December 19[16] and 2000 April 27,[17] respectively. On the basis of their broadband colors, both objects were identified as quasar candidates by the SDSS quasar target selection. SDSS spectroscopy on 2002 March 13 confirmed SDSS J1021+4913 to be a quasar at a redshift of $z = 1.72$[18] and on 2001 February 2 confirmed SDSS J1120+6711 to be a quasar at a redshift of $z = 1.49$.[19]

Having been confirmed as quasars, both objects were selected as lens candidates by the selection algorithm described by P03. This algorithm uses the point-spread function (PSF) as measured by the SDSS photometric pipeline (Lupton et al. 2001) to fit the postage stamp image of each $z > 0.6$ SDSS quasar to both a one- and a two-point-source model. Lens candidates, which are expected to exhibit multiple images, are required to show a significant improvement in goodness of fit when modeled with two point sources, as compared to one. Furthermore, selected candidates are required to have a best-fit component separation of $<3''$, to have a consistent geometry when fitted independently in g, r, and i, and to exhibit a color difference between quasar images not exceeding that allowed by a simple reddening model. Our two-PSF photometric models of the SDSS atlas images predicted for SDSS J1021+4913 a component separation of $1''.07$ and a flux ratio of A/B $\approx$ 2:1 and for SDSS J1120+6711 a component separation of $1''.75$ and a flux ratio of A/B $\approx$ 4:1. We further note that both candidates were also independently identified by the selection algorithm of Inada et al. (2005).

[16] The SDSS photometric designation of SDSS J1021+4913 is (run/rerun/camCol/field/ID) 2830/41/5/294/52.
[17] The SDSS photometric designation of SDSS J1120+6711 is (run/rerun/camCol/field/ID) 1412/40/4/131/6.
[18] The SDSS spectroscopic designation of SDSS J1021+4913 is (MJD/plate/fiber) 52347/873/560.
[19] The SDSS spectroscopic designation of SDSS J1120+6711 is (MJD/plate/fiber) 51942/491/431.

2.3. Spectroscopic Observations

We observed both objects on 2003 April 6, using the 6.5 m MMT. Spectra were obtained using the blue channel of the MMT spectrograph with the 300/mm grating and $1''$ slit, yielding a spectral resolution of 6 Å. The slit was aligned along the separation axis of the pairs, as predicted from SDSS imaging by a photometric model consisting of two point sources (see P03), so that the two components were observed simultaneously. The integration time was 600 s for SDSS J1021+4913 and 900 s for SDSS J1120+6711.

Although the seeing at the time of observation was approximately $1''$, the small separation between the quasar pairs led to their only being marginally resolved in the focal plane. Consequently, we implemented a deblending procedure to minimize cross-contamination between the extracted one-dimensional spectra. The spectra were deblended as follows:

1. The two-dimensional spectrum was binned into 20 bins along the dispersion axis, and the flux in each of these bins was integrated to produce a series of 20 spatial cross sections.
2. A profile consisting of two Gaussians was fitted to each of the spatial cross sections, subject to the constraint that the separation between the two Gaussians be the same for each bin.
3. Apertures for the two components were defined by assigning a fraction of the flux from each pixel to the first (second) aperture corresponding to the fractional contribution of the first (second) Gaussian to the model profile at that pixel. Hence, the model profiles can be thought of as relative weights that determine how much of the flux in a given pixel should be assigned to either of the two apertures.

This procedure is designed to ensure that the extracted apertures accurately trace the positions of the two objects on the two-dimensional image. However, for objects such as SDSS J1021+4913, for which the images of the two components overlap significantly in the focal plane, it cannot altogether eliminate cross-contamination. Fortunately, we can estimate and correct for the presence of contaminating flux as follows:

1. Two additional Gaussian models (sets of weights) are constructed, each of which is a spatial reflection of one of the original pair of Gaussian models with respect to the position of the other. For instance, the first reflected model is identical in shape to the first real model but appears on the other (spatial) side of the second real model.
2. Two reflected apertures are then assigned flux as above, using one reflected and one real set of weights for each. For instance, flux is assigned to the first reflected aperture using the first reflected and second real Gaussians.

Assuming that the PSF is essentially symmetric along the separation axis, these reflected apertures now contain the same amount of contaminating flux from the adjacent object as the real (unreflected) apertures. Cross-contamination can be corrected for by subtracting the flux in each reflected aperture from that in the corresponding real aperture. Figure 1 schematically illustrates our deblending procedure.

Figure 2 shows the spectra of the two components of SDSS J1021+4913. We cross-correlated the spectra and estimated the velocity difference between them to be less than the dispersion per pixel, corresponding to $\sim$100 km s^{-1}, and consistent with zero. The most significant spectral difference between the two components is that component B appears considerably redder at the blue end than component A. This qualitative assessment is supported by measurements of the equivalent widths of emission
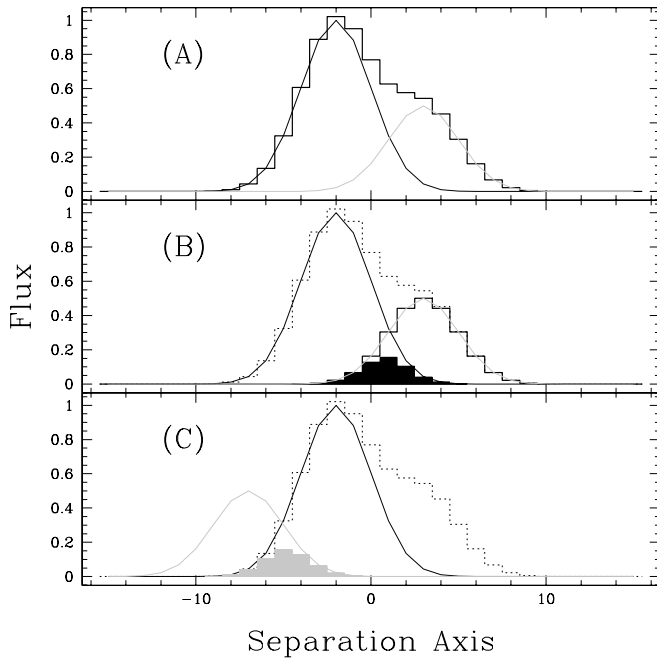
FIG. 1.—(a) Combined flux (*histogram*) of two marginally resolved sources along the separation axis. The two Gaussian curves represent the primary and secondary fitted weights. (b) Same as (a), but the combined flux is indicated by the dotted histogram. The flux assigned to the secondary aperture (*solid open histogram*) according to the two weights and the fraction of this assigned flux (*filled histogram*) that originates from the primary object are also shown. (c) The weight corresponding to the secondary object has been reflected onto the other side of the primary object, and flux has been assigned to a reflected aperture using this reflected and the original primary weight. The assigned flux (*shaded histogram*) is equal to, and can be used to correct for, the contaminating flux shown in (b).

lines in the two components [A: Lyα (450 ± 100 Å), C IV (400 ± 10 Å), and C III (105 ± 10 Å); B: Lyα (300 ± 50 Å), C IV (390 ± 30 Å), and C III (95 ± 10 Å)], although there are large uncertainties associated with determining an appropriate continuum level for Lyα. This discrepancy can be explained as being due to varying extinction along different sight lines through the lens galaxy. Note that the feature at 7600 Å is atmospheric.

Figure 3 shows the spectra of the two components of SDSS J1120+6711. We cross-correlated the spectra and also estimated
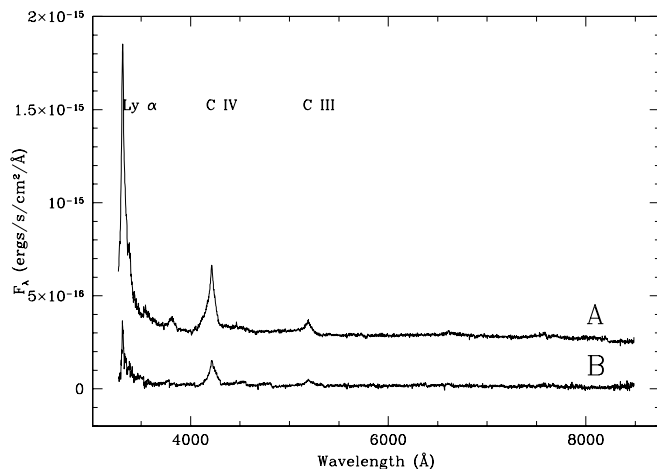

FIG. 2.—MMT spectra of the two components of SDSS J1021+4913. The spectrum of the brighter component has been shifted upward by an arbitrary offset to facilitate comparison.
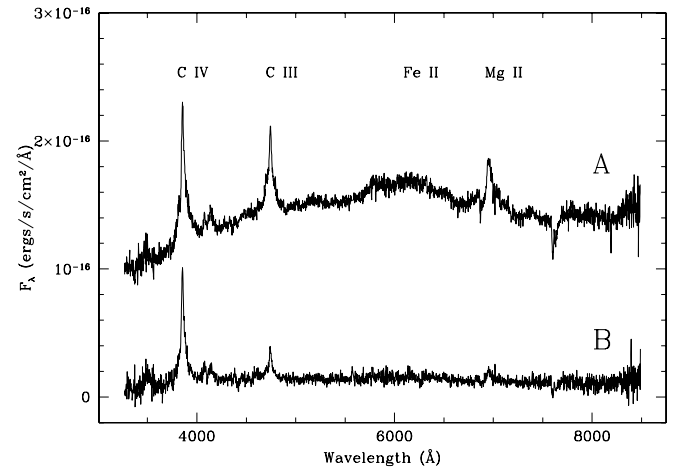

FIG. 3.—Same as Fig. 2, but for SDSS J1120+6711.

the velocity difference between them to be less than 100 km s^{-1}. The spectra of the two components differ significantly; the continuum of the brighter component is much redder at the blue end, the strength of the C IV line relative to the other lines is much greater in the fainter component, and there is no evidence of the fainter component of the broad Fe II complex that is seen blueward of Mg II in the brighter component.

In summary, spatially resolved spectroscopy revealed that both SDSS J1021+4913 and SDSS J1120+6711 are quasar pairs with indistinguishable redshifts. However, the two components of SDSS J1021+4913 have similar spectral energy distributions (SEDs), consistent with the lensing hypothesis, while the two components of SDSS J1120+6711 have significantly different SEDs.

2.4. *Near-IR Imaging*

We subsequently obtained near-infrared (near-IR) imaging of these two systems in order to search for the existence of a possible lens galaxy in each case.
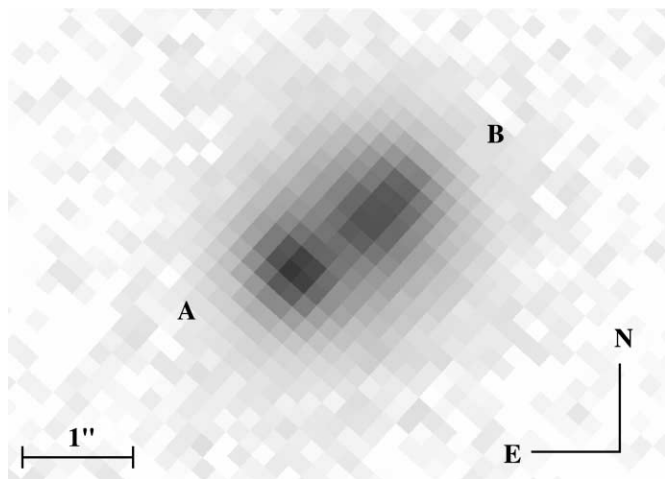
2.4.1. *SDSS J1021+4913*

On 2003 August 12, we imaged the system in the K' band using the Near Infrared Camera (NIRC; Matthews & Soifer 1994) on the Keck I telescope. The observations consisted of a five-point dither pattern, integrated for 30 s at each pointing. The data were flattened, sky subtracted, shifted, and stacked using the *dimsum* package in IRAF.

Figure 4 shows the K'-band image of SDSS J1021+4913. It is clear that the fainter component is extended relative to the brighter component. It is unlikely that this extended flux is associated with the quasar host galaxy, since (1) it would put the quasar at a very unusual off-center position relative to the host galaxy center of light and (2) it would be an additional coincidence that the host galaxy emission happens to be concentrated between the two quasars. Instead, we interpret this extended flux as indicating the presence of a lens galaxy. The lens galaxy is bright enough that it makes a simple PSF subtraction impractical. Hence, we modeled the system as a combination of three components: two point sources, using the profile recommended by Racine (1996), and an extended component represented by a de Vaucouleurs profile of the form

$$I(x, y) = I_0 \exp\left\{-7.67\left[(x^2 + y^2)^{1/2}/R_{\mathrm{eff}}\right]^{1/4}\right\} \quad (1)$$

FIG. 4.—NIRC K'-band image of SDSS J1021+4913.

TABLE 2
MASS MODELS FOR SDSS J1021+4913

Model	R_E (arcsec)	e or γ	θ_e or θ_γ (deg)[a]	Δt (h^{-1} day)[b]
SIS+shear	0.59	0.01	20.4	1.2
SIE	0.59	0.05	20.1	1.4

NOTE.—Derived from H-band photometry listed in Table 1.
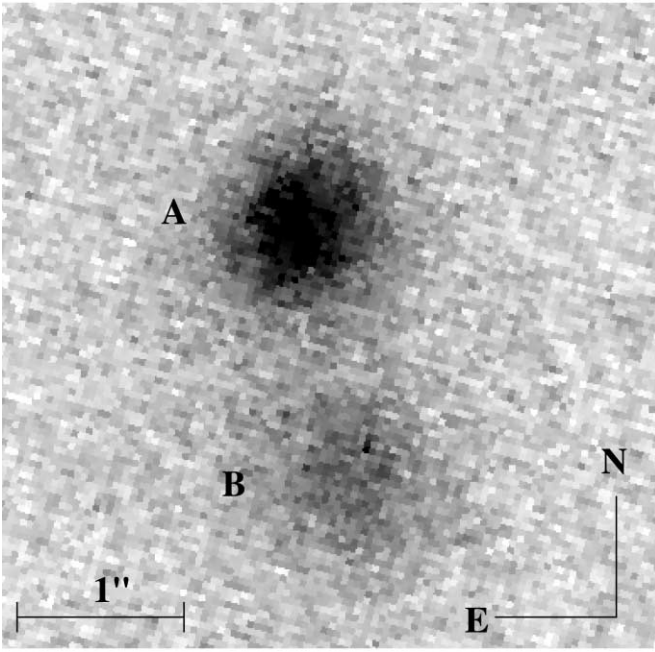[a] Each position angle is measured east of north.
[b] Positive time delays mean B leads A. We assumed a typical lens redshift of $z = 0.5$.

The best-fit photometric model indicates that the angular separation between quasar image A and the galaxy (AG) is nearly the same as that between B and the galaxy (BG). A simple singular isothermal sphere mass model, naturally, predicts that the quasar images should have nearly equal fluxes in this case. Instead, the observed flux ratio is A/B $\approx$ 5:2. This discrepancy can be explained by (1) extinction of image B relative to image A, consistent with the differential reddening noted above, or (2) modeling the lens galaxy with a more complicated mass distribution.

To explore the latter possibility, we modeled the lens system using two mass models: a singular isothermal sphere with external shear (SIS+shear) model and a singular isothermal ellipsoid (SIE) model. Each model has eight parameters: the Einstein radius R_E, shear or ellipticity (γ or e) and its position angle (θ_γ or θ_e), the position of the lens galaxy, the position of the source quasar, and the flux of the source quasar. The number of observables is also eight; therefore, the number of degrees of freedom is zero. We fit the mass models with the public software LENSMODEL (Keeton 2001). As expected, both models yield almost perfect fits, with χ^2 of $\sim$0. The resulting best-fit values are summarized in Table 2. We find that we can reproduce the photometric observations with mass models that have realistically small shear/ellipticity, $\gamma = 0.01$ or $e = 0.05$. Thus, the lensing hypothesis is also supported by our mass modeling of the system. We estimated the expected time delays between images and find that they are quite small, $\sim$1 h^{-1} day (B leads A), assuming a lens redshift of $z = 0.5$. This is because of the almost equal angular separation between AG and BG.

convolved with the PSF. In general, a de Vaucouleurs profile can also account for the axis ratio and position angle of a galaxy on the sky, but we chose this circularly symmetric form for simplicity. The parameters for the best-fit model are listed in Table 1. The uncertainties in this model are dominated by systematic errors associated with the imperfect PSF model. The errors listed are the observed variation in the model parameters when the best-fit FWHM is varied by $\pm$10%. The reduced χ^2 of the best-fit two-point-sources plus de Vaucouleurs model is 1.6 (1590 degrees of freedom [dof]). For comparison, the reduced χ^2 of the best-fit two-point-sources (only) model is 5.5 (1594 dof). We interpret this improvement in the fit as definitive evidence for the presence of a lens galaxy and, consequently, in support of the lensing hypothesis. There are no sources in the field bright enough to allow for direct calibration to Two Micron All Sky Survey photometry,[20] but we can use the results of K. R. Covey et al. (2006, in preparation), who characterized the stellar locus in optical and near-IR colors, to predict the K'-band magnitudes of SDSS-detected stars in the field. The errors in the derived magnitudes listed in Table 1 include the width of the stellar locus in the relevant optical-IR color space. However, we do not have enough data to characterize possible systematic errors in this photometric calibration, which may be significant compared to the random errors quoted.
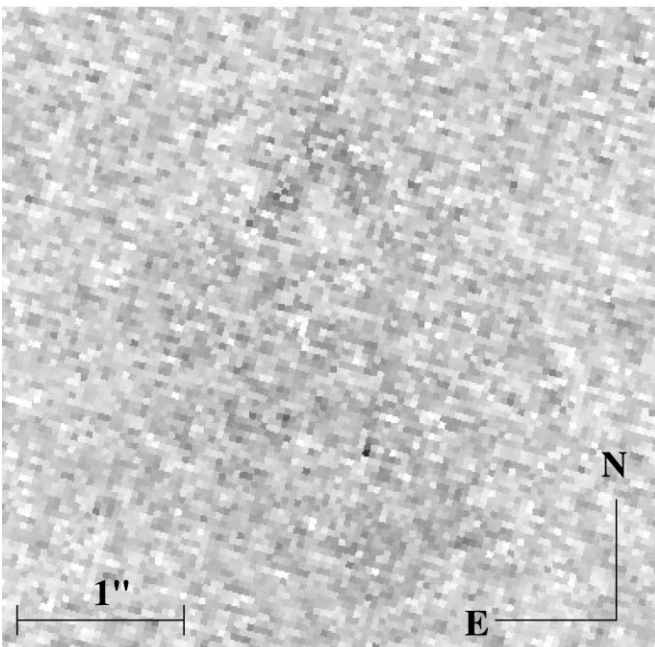
2.4.2. SDSS J1120+6711

On 2004 May 8, we imaged SDSS J1120+6711 in the H band at the MMT using the Arizona Infrared Imager and Echelle Spectrograph (ARIES) instrument (McCarthy et al. 1998) and

---

[20] Vizier Online Data Catalog, 2246 (R. M. Cutri et al.).

TABLE 1
PHOTOMETRIC MODEL PARAMETERS FOR SDSS J1021+4913

Parameter	Quasar A	Quasar B	Galaxy
H Band: Two Analytic PSFs Plus de Vaucouleurs			
Relative R.A. (arcsec)	0	-0.830 ± 0.029	-0.270 ± 0.003
Relative decl. (arcsec)	0	0.776 ± 0.029	0.514 ± 0.014
Relative flux[a]	1	0.38 ± 0.03	1.36 ± 0.43
Magnitude	18.4 ± 0.1	19.4 ± 0.1	18.0 ± 0.3
I Band: Two Analytic PSFs			
Relative R.A. (arcsec)	0	-0.796 ± 0.023	-0.499 ± 0.120
Relative decl. (arcsec)	0	0.784 ± 0.023	0.633 ± 0.120
Magnitude	19.02 ± 0.06	20.01 ± 0.10	21.72 ± 0.50

[a] Within measured effective radius.

Fig. 5.—ARIES H-band image of SDSS J1120+6711.

TABLE 3
Photometric Model Parameters for SDSS J1120+6711

Parameter	Quasar A	Quasar B
H Band: Two Analytic PSFs		
Relative R.A. (arcsec)............	0	-0.30 ± 0.02
Relative decl. (arcsec)............	0	-1.46 ± 0.02
Relative flux............................	1	0.42 ± 0.01
Magnitude	17.3 ± 0.1	18.3 ± 0.1
I Band: Two Analytic PSFs		
Relative R.A. (arcsec)............	0	-0.353 ± 0.008
Relative decl. (arcsec)............	0	-1.498 ± 0.008
Magnitude	18.49 ± 0.02	19.57 ± 0.04

the f/15 MMT-AO adaptive secondary (Riccardi et al. 2002). There is no guide star close enough to permit closed-loop imaging, but we used a bright star 12′ away to phase up the optical system. We integrated for 16 minutes before clouds rolled in. The resulting stack of images has a 0″.4 FWHM.

Figure 5 shows the H-band image of SDSS J1120+6711. The point sources appear extended because they are highly over-sampled by the minute pixel scale (0″.04), but there is no obvious indication of a lens galaxy. Indeed, a two-point-source model, again using the model profile of Racine (1996), fits the image very well, yielding a reduced χ^2 of 1.2 (6394 dof) and leaving residuals, shown in Figure 6, with no obvious flux concen-

trations. The parameters for this photometric model are listed in Table 3. Again, the magnitudes listed are derived by estimating the optical-IR colors of stars in the field from their SDSS colors.

Having subtracted the point sources, we set an upper limit on the flux of any remaining sources by introducing simulated point sources into the residual image and visually inspecting these simulated residuals. We thus estimated that any remaining sources could have a point-source flux of not more than 10% of the combined flux of components A and B. This upper limit corresponds to a magnitude of $H > 19.4 \pm 0.1$.

We can compare this upper limit to the results of Rusin et al. (2003), who found that the observed magnitudes of lens galaxies can be predicted from their observed image separations through the relation

$$m_{\mathrm{obs}} = M_{*0} + \mathrm{DM} + 2.5\gamma_{E+K}z_d - 1.25\gamma_{\mathrm{FJ}} \log \Delta\theta_{\mathrm{red}}, \quad (2)$$

where DM is the distance modulus, γ_{E+K} is a parameter subsuming evolution and spectral K-corrections, γ_{FJ} is the slope of the Faber-Jackson relation in the chosen band, z_d is the lens galaxy (deflector) redshift, and $\Delta\theta_{\mathrm{red}}$ is the reduced image separation, $\Delta\theta_{\mathrm{red}} \equiv (\Delta\theta/\Delta\theta_*)(D_s/D_{ds})$, where $\Delta\theta_*$ is the image separation produced by a singular isothermal sphere with a velocity dispersion of 225 km s^{-1} and D_s and D_{ds} are the angular diameter distances between the observer and source and the deflector and source, respectively. The H-band values of $M_{*0} = -23.8 + 5 \log h$, $\gamma_{E+K} = -0.21$, and $\gamma_{\mathrm{FJ}} = 3.32$ are all given by Rusin et al., based on *Hubble Space Telescope* photometry and spectrophotometric modeling of 28 early-type lens galaxies. The observed rms scatter is ∼0.5 mag. This relation predicts that given an observed source redshift and image separation, there exists a redshift at which the lens galaxy has a maximum apparent magnitude. In the case of SDSS J1120+6711, the maximum occurs at $z \sim 0.75$ and implies that $H < 18$. In short, we did not detect any indication of a lens galaxy in our H-band image of SDSS J1120+6711, and a simple estimate indicates that this nondetection is inconsistent with the presence of a lens galaxy of typical luminosity.

2.5. Optical Imaging

We further obtained deep I-band images of these two objects using the 8k mosaic CCD on the University of Hawaii 2.2 m telescope (UH88) at Mauna Kea. The imaging was conducted on 2004 May 23 (SDSS J1021+4913) and 25 (SDSS J1120+6711). The integration times were 120 s for SDSS J1120+6711 and 360 s for SDSS J1021+4913. We estimate the FWHM of these images to be 0″.8. Note that the optical and near-IR images

Fig. 6.—The H-band residuals for SDSS J1120+6711 following subtraction of two point sources. The gray scale is the same as in Fig. 5.
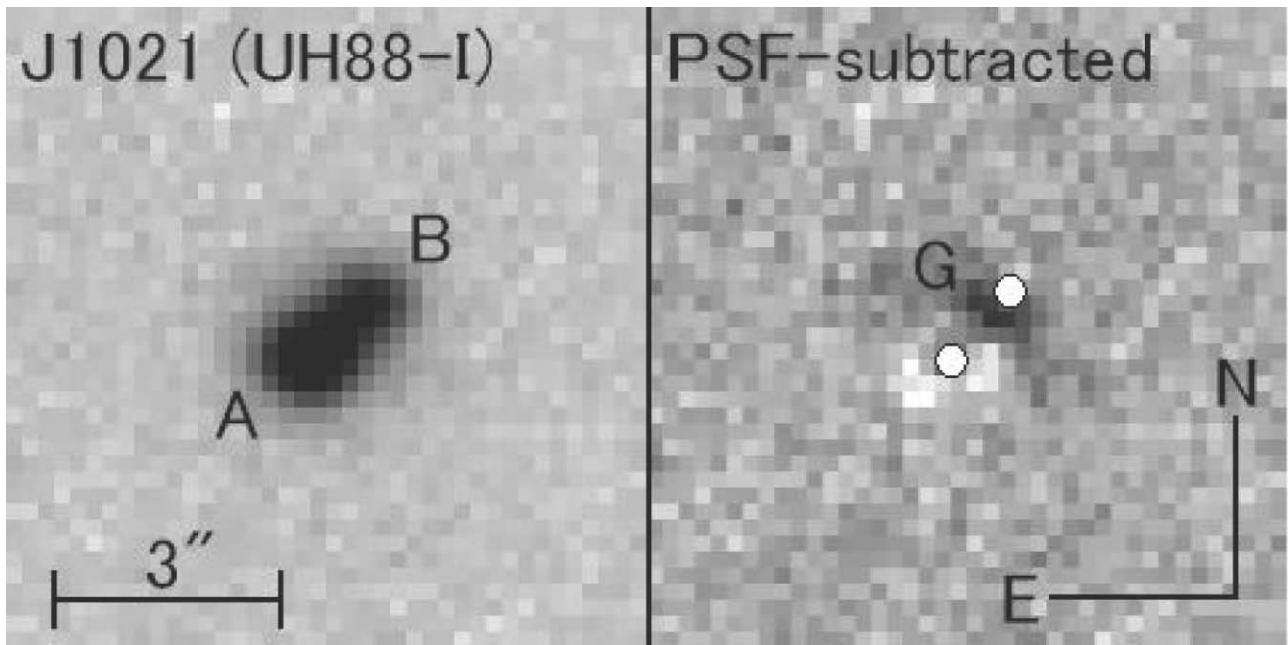
Fig. 7.—UH88 *I*-band image of SDSS J1021+4913. The white dots in the PSF-subtracted image indicate the location of the point-source components.

were independently analyzed by two of the authors, N. Inada and B. Pindor, respectively, and discrepancies between the photometric models are most likely indicative of the systematic errors present.

2.5.1. *SDSS J1021+4913*

Figure 7 shows the *I*-band image of SDSS J1021+4913, both as observed and following the subtraction of two point sources. For the optical data, the point-source subtraction was performed using a Gaussian PSF model whose FWHM was determined by fitting to nearby stars. Table 1 lists the corresponding photometric model. Photometric calibration was obtained relative to the standard star PG 1528+062 (Landolt 1992). The listed magni-

tude errors do not include the photometric uncertainty of the standard star. We take the close agreement between our optical and near-IR models as definitive confirmation of the presence of the lens galaxy. Certainly, the derived galaxy magnitude makes this object too bright to be a $z = 1.72$ host galaxy (Daddi et al. 2005). We can invert the relation of Rusin et al. (2003) to estimate the lens galaxy redshift, but the derived constraint, $0.45 < z < 1.25$ (66% confidence), is not very stringent.

2.5.2. *SDSS J1120+6711*

Figure 8 shows the *I*-band image of SDSS J1120+6711, both as observed and following the subtraction of two point sources. Table 3 lists the corresponding photometric model. We are
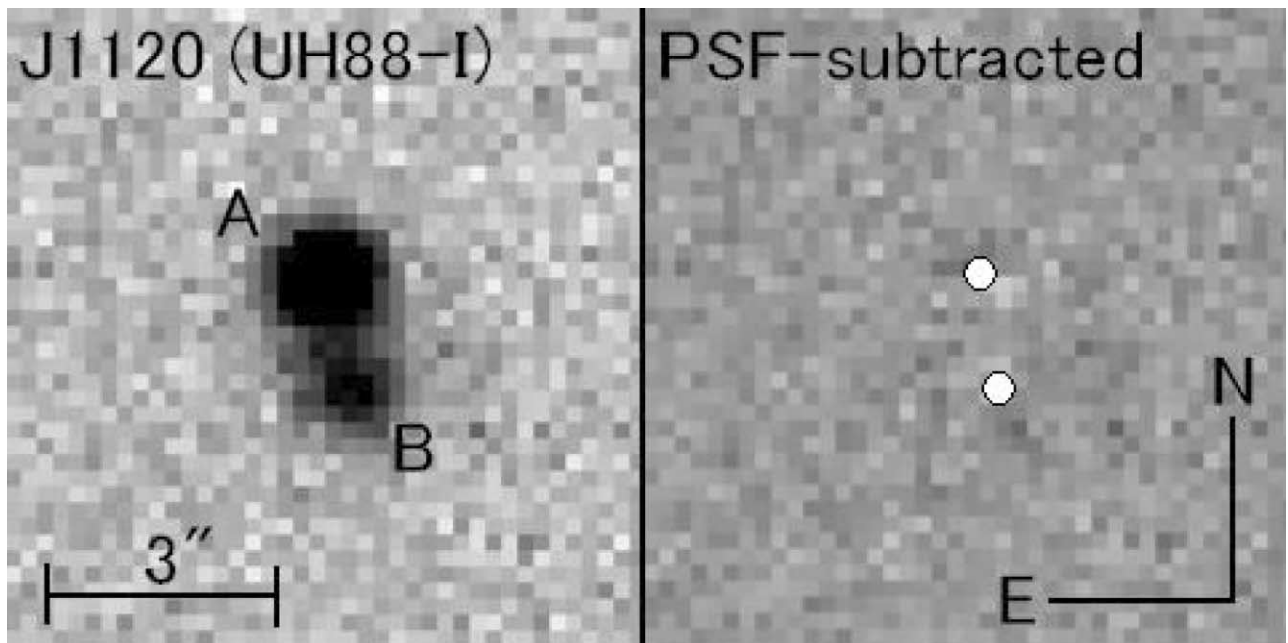

Fig. 8.—Same as Fig. 7, but for SDSS J1120+6711.

unable to detect any object in the residual image corresponding to more than a 3 σ fluctuation above the sky level. We estimate that this corresponds to an upper limit of $I > 24$. Again employing the method of Rusin et al. (2003), we predict that the I-band magnitude of the lens galaxy should be $I < 20.5$. In agreement with our H-band image, the I-band image of SDSS J1120+6711 shows no evidence of a lens galaxy and is inconsistent with the presence of a lens galaxy of typical luminosity.

3. CONCLUSIONS

The observations reported above have confirmed that SDSS J102111.02+491330.4 is almost certainly a previously unknown gravitationally lensed quasar. High spatial resolution spectroscopy revealed the existence of two quasar images with an angular separation of $1\rlap{.}''14 \pm 0\rlap{.}''04$ and having identical redshifts of $z = 1.72$. High-resolution K'-band imaging indicates the presence of a lens galaxy between the two quasar images. SDSS J1021+4913 does not appear to have any peculiarities that would obviously compel individual studies of the system. Conversely, the fact that simple lens models readily reproduce the lens geometry implies that the system is well suited to various ensemble studies. The utility of this system in such studies would be aided by an improved photometric characterization and optical redshift measurement of the lens galaxy, both of which should be plausible for an 8 m class telescope. Our mass models predict a short time delay ($\sim$1 day), but the relatively small separation of the two quasar images makes the system less than ideal for a monitoring campaign. SDSS J1021+4913 represents an incremental increase in what will likely soon be the largest uniformly selected sample of lensed quasars. The SDSS lens sample will have an additional merit relative to radio surveys like CLASS in that both the redshifts of the lensed sources are known and the redshift distribution of the background quasar population is well characterized (Richards et al. 2005).

Observations of SDSS J112012.12+671116.0 indicate that it is more likely a binary quasar than a lensed pair. Although the two components are both quasars with indistinguishable redshifts of $z = 1.49$, they have markedly different SEDs. Optical and H-band imaging of the system did not reveal any indication of a lens galaxy. Binary quasars can be considered a contaminant in a search for gravitational lenses, but they are interesting objects in their own right. The SDSS has previously discovered a number of other binary quasars, although mostly, due to fiber

collisions, at considerably greater angular separations (Schneider et al. 2003). A sample of SDSS-selected binary quasars will provide insights on quasar clustering and the onset of the quasar phenomenon (Hennawi et al. 2006). It has been known for some time that extrapolating observed large-scale quasar-quasar clustering to small separations considerably underpredicts the number of arcsecond-scale binaries (Djorgovski 1991). Hence, the confirmation of SDSS J1120+6711 and other uniformly selected binaries is the best empirical method for determining the binary to lens ratio at these separations. Knowledge of this ratio is important for trying to predict the efficiency of future lens searches (Pindor 2005).

APPENDIX

REJECTED LENS CANDIDATES

The program of follow-up observations that confirmed the lensing nature of SDSS J1021+4913 and several previous SDSS-identified gravitational lenses also served to reject the lensing hypothesis for numerous objects. Table 4 lists the positions of these rejected lens candidates. Typically, spatially resolved spectroscopy has shown these objects to be quasar plus star superpositions. For objects that are not commented, we are unable to confidently identify the nature of the secondary object, but we can rule out the presence of broad quasar emission lines matching those of the primary object. The one binary quasar listed, SDSS J1600+0000, has an obvious redshift difference. We have indicated those objects that satisfy the selection criteria of P03. Those objects that do not satisfy the P03 selection were either observed prior to finalization of the algorithm, selected by an altogether different algorithm, or were marginal candidates that were chosen due to observing conditions. From this list, we can surmise that quasar plus star superpositions dominate the population of false positives in this optical search and that, compared to the >10 lenses that have been discovered or were previously known in the parent sample, the number of binaries is considerably smaller than the number of lenses at separations of $1''$–$3''$. This is not an exhaustive list of those lens candidates that we have observed but rather a list of those candidates that we are confident do not merit further observation in the context of lensing investigations. It should not in any way be taken as a statistical complement to the list of published SDSS lenses. Instead, our main motivation in publishing this list is to inform other investigators who might independently select these objects as lens candidates of the results of these observations. Additional photometric and spectroscopic data for these objects are available through the SDSS SkyServer.

PINDOR ET AL.

TABLE 4
Positions of Rejected SDSS Lens Candidates

R.A.	Decl.	P03	Comment
08 24 04.42	+37 18 54.7	Y	QSO + ELG
08 45 12.73	+54 34 21.5	Y	QSO + star?
10 11 26.67	+00 43 19.2	N	Ruled out by imaging
10 30 21.94	+58 55 13.9	Y	QSO + ELG
10 41 22.84	−00 56 18.5	N	QSO + star
11 12 25.73	−00 51 01.6	N	
11 36 13.39	+03 38 41.1	Y	QSO + star
12 14 05.13	+01 02 05.0	N	
12 51 41.91	+03 11 40.9	Y	QSO + star
13 08 54.29	−02 36 13.4	N	
13 39 04.34	+00 22 22.1	Y	
14 33 16.39	+00 51 45.7	Y	QSO + star
14 34 52.73	−00 28 28.1	Y	QSO + gal.?
14 41 45.10	+02 37 43.3	Y	QSO + star
14 46 19.29	+00 53 17.9	N	
15 08 24.22	−00 06 03.9	Y	
15 12 36.94	+55 39 01.4	Y	QSO + WD?
15 15 38.95	−00 12 40.8	N	
15 21 19.68	−00 48 18.7	N	
15 25 55.81	+01 08 35.5	N	QSO + star
15 30 28.56	+51 15 14.4	Y	QSO + QSO?
15 41 07.46	−00 37 16.1	Y	QSO + star
16 00 15.51	+00 00 45.5	Y	Binary quasar, $z = 1.01$, $\Delta z = 0.003$, angular separation $1\rlap{.}''8$
16 05 12.00	−00 47 49.6	Y	QSO + star
16 24 15.28	+00 32 51.1	Y	QSO + WD?
17 17 47.57	+59 32 58.2	N	
17 23 08.15	+52 44 55.5	Y	QSO + star
17 24 06.47	+64 07 10.7	N	
17 25 50.89	+56 58 59.9	Y	
21 29 06.24	−07 16 13.3	Y	QSO + star
23 11 16.98	−10 38 49.7	Y	QSO + star

Note.—Units of right ascension are hours, minutes, and seconds, and units of declination are degrees, arcminutes, and arcseconds.

REFERENCES

Abazajian, K., et al. 2003, AJ, 126, 2081
———. 2004, AJ, 128, 502
———. 2005, AJ, 129, 1755
Blanton, M. R., Lin, H., Lupton, R. H., Maley, F. M., Young, N., Zehavi, I., & Loveday, J. 2003, AJ, 125, 2276
Chae, K.-H., & Mao, S. 2003, ApJ, 599, L61
Chae, K.-H., et al. 2002, Phys. Rev. Lett., 89, 151301
Cohn, J. D., & Kochanek, C. S. 2004, ApJ, 608, 25
Daddi, E., et al. 2005, ApJ, 626, 680
Djorgovski, S. 1991, in ASP Conf. Ser. 21, The Space Distribution of Quasars, ed. D. Crampton (San Francisco: ASP), 349
Fukugita, M., Futamase, T., & Kasai, M. 1990, MNRAS, 246, 24P
Fukugita, M., Ichikawa, T., Gunn, J. E., Doi, M., Shimasaku, K., & Schneider, D. P. 1996, AJ, 111, 1748
Gunn, J. E., et al. 1998, AJ, 116, 3040
Hennawi, J. F., et al. 2006, AJ, 131, 1
Hogg, D. W., Finkbeiner, D. P., Schlegel, D. J., & Gunn, J. E. 2001, AJ, 122, 2129
Inada, N., et al. 2003, Nature, 426, 810
———. 2005, AJ, 130, 1967
Ivezić, Ž., et al. 2002, AJ, 124, 2364
———. 2004, Astron. Nachr., 325, 583
Johnston, D. E., et al. 2003, AJ, 126, 2281
Keeton, C. R. 2001, preprint (astro-ph/0102340)
Kochanek, C. S. 1995, ApJ, 445, 559
Kochanek, C. S., Schneider, P., & Wambsganss, J. 2006, in Part 2 of Gravitational Lensing: Strong, Weak & Micro, Proc. 33rd Saas-Fee Advanced Course, ed. G. Meylan, P. Jetzer, & P. North (Berlin: Springer), in press (astro-ph/0407232)
Koopmans, L. V. E., & Fassnacht, C. D. 1999, ApJ, 527, 513
Kuhlen, M., Keeton, C. R., & Madau, P. 2004, ApJ, 601, 104

Kundic, T., et al. 1997, ApJ, 482, 75
Landolt, A. U. 1992, AJ, 104, 340
Li, L., & Ostriker, J. P. 2002, ApJ, 566, 652
Lupton, R. H., Gunn, J. E., Ivezić, Ž., Knapp, G. R., Kent, S., & Yasuda, N. 2001, in ASP Conf. Ser. 238, Astronomical Data Analysis Software and Systems X, ed. F. R. Harnden, Jr., F. A. Primini, & H. E. Payne (San Francisco: ASP), 269
Matthews, K., & Soifer, B. T. 1994, Exp. Astron., 3, 77
McCarthy, D. W., Burge, J. H., Angel, J. R. P., Ge, J., Sarlot, R. J., Fitz-Patrick, B. C., & Hinz, J. L. 1998, Proc. SPIE, 3354, 750
Myers, S. T., et al. 2003, MNRAS, 341, 1
Pier, J. R., Munn, J. A., Hindsley, R. B., Hennessy, G. S., Kent, S. M., Lupton, R. H., & Ivezić, Ž. 2003, AJ, 125, 1559
Pindor, B. 2005, ApJ, 626, 649
Pindor, B., Turner, E. L., Lupton, R. H., & Brinkmann, J. 2003, AJ, 125, 2325 (P03)
Pindor, B., et al. 2004, AJ, 127, 1318
Racine, R. 1996, PASP, 108, 699
Refsdal, S. 1964, MNRAS, 128, 307
Riccardi, A., et al. 2002, in Beyond Conventional Adaptive Optics, ed. E. Vernet et al. (Garching: ESO), 55
Richards, G. T., et al. 2002, AJ, 123, 2945
———. 2005, MNRAS, 360, 839
Rusin, D., & Kochanek, C. S. 2005, ApJ, 623, 666
Rusin, D., et al. 2003, ApJ, 587, 143
Schneider, D. P., et al. 2003, AJ, 126, 2579
Smith, J. A., et al. 2002, AJ, 123, 2121
Stoughton, C., et al. 2002, AJ, 123, 485
Treu, T., & Koopmans, L. V. E. 2004, ApJ, 611, 739
Turner, E. L. 1990, ApJ, 365, L43
York, D. G., et al. 2000, AJ, 120, 1579